

Structure-based ligand discovery for the Large-neutral Amino Acid Transporter 1, LAT-1

Ethan G. Geier^{a,1}, Avner Schlessinger^{a,b,1,2}, Hao Fan^{a,b,c}, Jonathan E. Gable^{c,d}, John J. Irwin^{a,b,c}, Andrej Sali^{a,b,c,3}, and Kathleen M. Giacomini^{a,3}

Departments of ^aBioengineering and Therapeutic Sciences and ^cPharmaceutical Chemistry, ^bCalifornia Institute for Quantitative Biosciences, and ^dGraduate Group in Biophysics, University of California, San Francisco, CA 94158

Edited by John Kuriyan, University of California, Berkeley, CA, and approved February 19, 2013 (received for review October 17, 2012)

The Large-neutral Amino Acid Transporter 1 (LAT-1)—a sodium-independent exchanger of amino acids, thyroid hormones, and prescription drugs—is highly expressed in the blood–brain barrier and various types of cancer. LAT-1 plays an important role in cancer development as well as in mediating drug and nutrient delivery across the blood–brain barrier, making it a key drug target. Here, we identify four LAT-1 ligands, including one chemically novel substrate, by comparative modeling, virtual screening, and experimental validation. These results may rationalize the enhanced brain permeability of two drugs, including the anticancer agent acivicin. Finally, two of our hits inhibited proliferation of a cancer cell line by distinct mechanisms, providing useful chemical tools to characterize the role of LAT-1 in cancer metabolism.

membrane transporter | polypharmacology | glioblastoma multiforme | solute carrier (SLC) transporter

Large-neutral Amino Acid Transporter 1 (LAT-1) is a sodium-independent exchanger found in the brain, testis, and placenta, where it mediates transport of large-neutral amino acids (e.g., tyrosine) and thyroid hormones (e.g., triiodothyronine) across the cell membrane (1). More specifically, LAT-1 is highly expressed in the blood- and brain-facing membranes of the blood–brain barrier (BBB) to supply the central nervous system (CNS) with essential nutrients and to help maintain the neural microenvironment (2). LAT-1 is also an important drug target because it transports several prescription drugs, such as the antiparkinsonian drug L-dopa and the anticonvulsant gabapentin, across the BBB, thereby enabling their pharmacologic effects (3, 4). This function at the BBB has made LAT-1 a target for drug delivery by modifying CNS-impermeable drugs such that they become LAT-1 substrates and have enhanced BBB penetration (5, 6).

In addition, LAT-1 expression levels are increased in many types of cancer, including non-small-cell lung cancer and glioblastoma multiforme (GBM) (7, 8). LAT-1 expression increases as cancers progress, leading to higher expression levels in high-grade tumors and metastases (9). In particular, LAT-1 plays a key role in cancer-associated reprogrammed metabolic networks by supplying growing tumor cells with essential amino acids that are used as nutrients to build biomass and signaling molecules to enhance proliferation by activating progrowth pathways such as the mammalian target of rapamycin (mTOR) pathway (10). Furthermore, inhibiting LAT-1 function reduces tumor cell proliferation, indicating that it may be a viable target for novel anticancer therapies (11–13). A cancer drug targeting LAT-1 can therefore be a LAT-1 inhibitor that deprives the cancer cells of nutrients or a cytotoxic LAT-1 substrate with an intracellular target (e.g., a metabolic enzyme).

LAT-1 is a large protein with 12 putative membrane-spanning helices (14). To transport solutes across the membrane, LAT-1 binds SLC3A2, a glycoprotein with a single membrane-spanning helix that serves as a chaperone for LAT-1 (14). The atomic structure of human LAT-1 is not known, but LAT-1 exhibits significant sequence similarity to prokaryotic transporters such as members of the amino acid/polyamine/organocation transporter (APC) family, whose representative structures have been recently

determined by X-ray crystallography (15–19). Structures of the arginine:agmatine antiporter AdiC from *Escherichia coli* (15, 17, 18) and *Salmonella enterica* (20) in different conformations reveal an internal twofold pseudosymmetry, similar to the structures of the sodium- and chloride-dependent leucine transporter, LeuT (19, 21). These data, combined with structures of additional related transporters (22) and molecular dynamics (MD) simulations (23), suggest a common transport mechanism among the LAT-1 homologs and LeuT, in which the role of sodium in LeuT is proposed to be mimicked by a proton in some APC transporters (23). Thus, LAT-1 probably also transports ligands across the cell membrane via the alternating access transport mechanism (22, 24, 25).

In this study, we take an integrated computational and experimental approach to characterize previously unknown LAT-1 ligands. We construct structural models of LAT-1 based on structures of homologous APC family transporters from prokaryotic organisms and then perform virtual ligand screening of metabolite and prescription drug libraries against these models to predict small-molecule ligands. The top-scoring hits are tested experimentally for LAT-1 inhibition and transport by using *cis*-inhibition experiments and *trans*-stimulation assays, respectively. Furthermore, we characterize the effect of select validated ligands on cell proliferation. Finally, we describe the pharmacological implications of our results, including how the intended and unintended effects of the discovered ligands may be mediated by LAT-1 transport across the BBB as well as their potential use as chemical tools to characterize the role of LAT-1 in cancer.

Results

LAT-1 Predicted Structure and Ligand Binding. LAT-1 was modeled based on the X-ray structure of the arginine:agmatine transporter AdiC from *E. coli* in the outward-occluded arginine-bound conformation (17) and the structure of the APC transporter ApcT from *Methanococcus jannaschii* in an inward-*apo* conformation (16) (Fig. S1 and *SI Materials and Methods*). The final LAT-1 model contains the whole transmembrane domain of the protein (i.e., the 12 transmembrane helices), including the residues constituting the predicted ligand-binding site. Comparative models were first scored by using Z-DOPE, a normalized atomic distance-dependent statistical potential based on known protein structures (26). The Z-DOPE scores of the top models were -0.3 , suggesting that 60% of its C α atoms are within 3.5 Å of their correct positions

Author contributions: E.G.G., A. Schlessinger, J.J.I., A. Sali, and K.M.G. designed research; E.G.G., A. Schlessinger, and J.E.G. performed research; E.G.G., A. Schlessinger, A. Sali, and K.M.G. contributed new reagents/analytic tools; E.G.G., A. Schlessinger, H.F., J.E.G., A. Sali, and K.M.G. analyzed data; and E.G.G., A. Schlessinger, A. Sali, and K.M.G. wrote the paper.

The authors declare no conflict of interest.

This article is a PNAS Direct Submission.

¹E.G.G. and A. Schlessinger contributed equally to this work.

²Present address: Department of Pharmacology and Systems Therapeutics, Tisch Cancer Center, Mount Sinai School of Medicine, New York, NY 10029.

³To whom correspondence may be addressed. E-mail: sali@salilab.org or kathy.giacomini@ucsf.edu.

This article contains supporting information online at www.pnas.org/lookup/suppl/doi:10.1073/pnas.1218165110/-DCSupplemental.

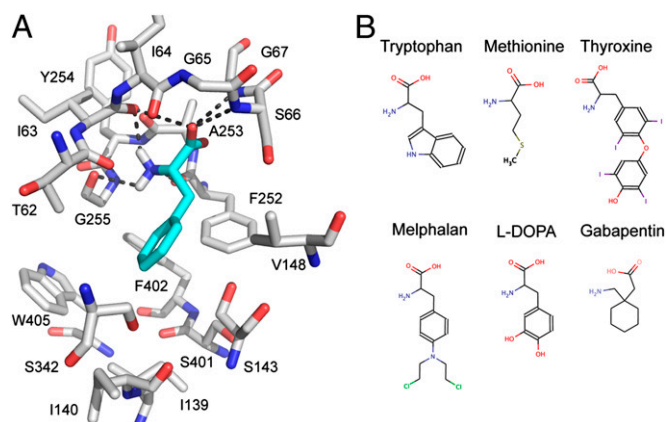


Fig. 1. Predicted LAT-1 structure and ligand-binding mode. (A) Predicted structure of the LAT-1-phenylalanine complex. LAT-1 (gray) and phenylalanine (cyan) are shown as the stick models; oxygen, nitrogen, and hydrogen atoms are depicted in red, blue, and white, respectively; key hydrogen bonds between phenylalanine and LAT-1 (involving residues Thr-62, Ile-63, Ile-64, Ser-66, Gly-67, Phe-252, Ala-253, and Gly-255) are shown as dotted gray lines. (B) Structures of representative LAT-1 substrates. Known LAT-1 substrates, including metabolites (tryptophan, methionine, and thyroxine) and prescription drugs (melphalan, L-dopa, and gabapentin) are shown using MarvinView 5.4.1.1 (Chemaxon).

(27) (Table S1). Each model was also evaluated based on its ability to discriminate between known ligands and likely nonbinders (decoys), by using enrichment curves derived from ligand-docking calculations (28). The logAUC score for the final refined LAT-1 model was 31.9 (Table S1), suggesting that it is suitable for predicting ligands for experimental testing (28–30).

The model of LAT-1 interacting with phenylalanine indicates that the majority of the key polar interactions between LAT-1 and the carboxyl and amino group of the amino acid ligands are conserved between LAT-1 and the AdiC template structure (Fig. 1A and Fig. S1). For example, the backbone polar groups of LAT-1 residues T62, I63, I64, S66, G67, F252, A253, and G255 are predicted to form polar interactions with phenylalanine (Fig. 1). These residues correspond to A22, I23, M24, S26, G27, W202, S203, and I205 of AdiC, which make similar interactions with the carboxyl and amino groups of its ligand arginine (17). Because the carboxyl and amino groups are conserved among all other known LAT-1 ligands, such as thyroxine and gabapentin (Fig. 1B), we hypothesize that they make similar interactions with LAT-1.

Conversely, differences in the ligand preferences of LAT-1 and AdiC may be explained by two major differences in the binding sites of the LAT-1 model and the AdiC structure (Fig. S2). First, several residues with hydrophobic side chains (i.e., I139, V148, F252, F402, and W405) are located in the LAT-1 binding site, likely contributing to increased ligand-binding affinity of hydrophobic amino acids to LAT-1 via van der Waals interactions and the hydrophobic effect (e.g., the tryptophan indole ring). Some of these hydrophobic residues are replaced by nonhydrophobic residues in LAT-1 homologs, including the template structure AdiC and other SLC7 members. For instance, the aromatic residue W405 in LAT-1 corresponds to the polar T361 in AdiC. Second, several binding site residues in AdiC are replaced by residues with smaller side chains in LAT-1, creating a larger volume in LAT-1's binding site that can accommodate larger amino acids. For instance, M104, I205, and W293 in AdiC correspond to the smaller V148, G255, and S342 in LAT-1 (Fig. 1A and Fig. S2).

Virtual Screening of Drugs and Metabolites. We computationally screened filtered libraries of 6,436 and 12,730 small molecules from the Kyoto Encyclopedia of Genes and Genomes (KEGG) DRUG and KEGG LIGAND COMPOUND databases (28), respectively, against two LAT-1 models (Fig. 2 and Table S1).

Some of the top-scoring hits were shown previously to be LAT-1 ligands, increasing our confidence in the binding site model. For example, the known substrate L-Trp was ranked 50th in the docking screen of KEGG LIGAND COMPOUND. The 200 (3.1%) KEGG DRUG and 500 (3.9%) KEGG COMPOUND top-scoring hits against our top two models were analyzed manually. A compound was selected for experimental testing based on three criteria: (i) similarity between its docking pose and those of known ligands in complex with LAT-1 (28); (ii) the chemical novelty of its scaffold, especially if it occurred frequently among the top-scoring compounds; and (iii) its pharmacological effect (28).

Experimental Validation of Predicted Ligands. A LAT-1-overexpressing cell line was generated by stably transfecting HEK cells with human LAT-1 cDNA. HEK-LAT1 cells expressed 20-fold higher levels of LAT-1 mRNA relative to HEK-EV cells and demonstrated LAT-1-specific uptake of the established system L substrates, gabapentin and L-leucine (Fig. S3A–D). Twelve of the top-scoring molecules were selected for experimental testing by *cis*-inhibition assay (Table 1, Table S2, and Fig. 2). Each molecule was tested as a LAT-1 ligand by determining its ability to inhibit transport of a known LAT-1 substrate in HEK-LAT1 cells at concentrations of 10 and 100 μ M (Fig. 3 and Fig. S3E). The known LAT-1 inhibitor 2-aminobicyclo-(2,2,1)-heptane-2-carboxylic acid (BCH) was also included as a positive control. At 100 μ M, inhibition of intracellular gabapentin accumulation ranged from 88% (3,5-diiodo-L-tyrosine) to <10% (cystine, mebendazole, and nocaedazole), with the metabolites 3,5-diiodo-L-tyrosine and 3-iodo-L-tyrosine, as well as the tryptophan hydroxylase inhibitor fenclonine and the anticancer agent acivicin, demonstrating significant inhibition of gabapentin and L-leucine transport (Fig. 3A and Fig. S3E). Acivicin also obtained a dissimilarity score of 0.74 using the JCDissimilarityCFTanimoto score, which calculates dissimilarities among molecules based on chemical fingerprints,

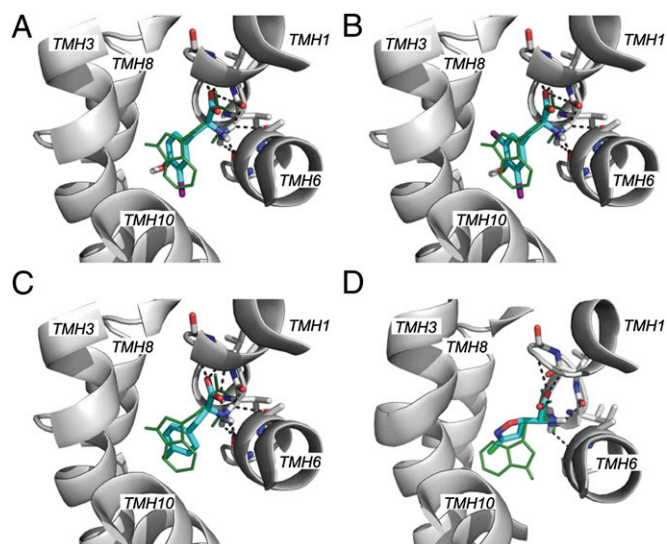
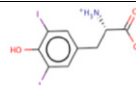
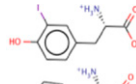
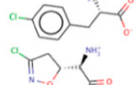
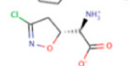


Fig. 2. Predicted binding modes for LAT-1 ligands. Predicted binding modes of the known substrate tryptophan (green lines) and four ligands discovered in the docking screen. Residues making polar interactions with the ligand are illustrated with sticks; carbon atoms are colored in white, nitrogen atoms in blue, and oxygen atoms in red; hydrogen bonds are represented by dotted gray lines. The predicted pose of a known LAT-1 ligand, tryptophan, is shown with green lines. The compounds depicted are 3-iodo-L-tyrosine (A), 3,5-diiodo-L-tyrosine (B), fenclonine (C), and acivicin (D). Halogen atoms in the discovered ligands are colored in purple (iodine) and green (chlorine).

Table 1. Small-molecule ligands confirmed experimentally

| Name* | Function† | Dissimilarity‡ | Sketch§ |
|----------------------|--|----------------|---|
| 3,5-I-diiodotyrosine | Tyrosine metabolism; thyroid hormone deficiency treatment; radioactive agent | 0.26 |  |
| 3-Iodo-L-tyrosine | Tyrosine metabolism; radioactive agent | 0.23 |  |
| Fenclonine | Serotonin inhibitor | 0.18 |  |
| Acivicin | Antineoplastic | 0.74 |  |

*Generic or chemical name of the molecule.

†Pharmacological function of the drug or the physiological function of the metabolites, when applicable.

‡Dissimilarity measure calculated with the Chemaxon fingerprints. Dissimilarity values of >0.7 suggest that the molecule is chemically different from all known LAT-1 ligands.

§A 2D sketch of the molecule is shown.

indicating that it is a chemically novel LAT-1 ligand (Table 1 and *Materials and Methods*).

The potencies of selected active ligands were further established by determining the IC₅₀ values for inhibiting gabapentin accumulation in the HEK-LAT1 cells. IC₅₀ values ranged from 7.9 μ M (3,5-diiodo-L-tyrosine; Fig. 3*B*) to 340 μ M (acivicin; Fig. 3*C*). At 10 μ M, inhibition of gabapentin accumulation ranged

from 61% (3,5 diiodo-L-tyrosine) to <10%, with 3,5-diiodo-L-tyrosine and 3-iodo-L-tyrosine significantly inhibiting gabapentin transport (Fig. 3*A*). Interestingly, 3,5-diiodo-L-tyrosine is a stronger inhibitor than the positive control BCH. In summary, one-third (4 of 12) of the top-scoring molecules selected for experimental testing are LAT-1 ligands capable of inhibiting gabapentin and L-leucine transport in HEK-LAT1 cells.

Identification of LAT-1 Substrates. The four molecules found to significantly inhibit gabapentin accumulation in the HEK-LAT1 cells were further analyzed as putative substrates by *trans*-stimulation assay. This assay takes advantage of LAT-1's obligatory exchange mechanism of transport by exchanging intracellular L-leucine from preloaded HEK-LAT1 cells with an extracellular molecule only if it is a LAT-1 substrate. Three known LAT-1 substrates served as positive controls and were able to induce L-leucine efflux from the HEK-LAT1 cells, including L-leucine (43%), gabapentin (36%), and BCH (30%) (Fig. 4*A*). In contrast, glycine was used as a negative control because it is known not to be a LAT-1 substrate and did not induce any L-leucine efflux. Two of the four inhibitors confirmed in our *cis*-inhibition assay also induced L-leucine efflux. Acivicin and fenclonine induced L-leucine efflux by 27% and 29%, respectively, indicating that they are transported by LAT-1. These results indicate that the drug-like molecules acivicin and fenclonine, which both have pharmacodynamic effects in the CNS, are likely LAT-1 substrates. Surprisingly, both of the more potent LAT-1 inhibitors, the metabolites 3,5-diiodo-L-tyrosine and 3-iodo-L-tyrosine, were only able to induce 7.9% and 5.4% L-leucine efflux, respectively, suggesting that they are inhibitors that only bind to, but are not transported by, LAT-1. Finally, guanfacine and rufinamide were also studied, and neither induced significant L-leucine efflux.

Inhibition of LAT-1-Dependent Cell Proliferation. LAT-1 is highly expressed in various cancer cells, providing them with nutrients and signaling molecules for growth. Thus, a drug targeting LAT-1 in cancer can be an inhibitor that deprives the cancer cells from nutrients or a cytotoxic substrate with an intracellular target. We therefore investigated the antiproliferative effects of select validated LAT-1 ligands, including the LAT-1 substrate acivicin and the inhibitor 3-iodo-L-tyrosine, by cell proliferation assay in the high LAT-1-expressing GBM cell line, T98G (8). The LAT-1-specific effects of each ligand on cell growth were determined in control cells (T98G-EV) and cells with LAT-1 expression (Fig. S4*A*) and function (Fig. S4*B*) knocked down (T98G-KD). The anticancer drug acivicin was a more potent growth inhibitor of T98G-EV (75% growth reduction) than T98G-KD (51% growth reduction) (Fig. 4*B*). Similarly, 3-iodo-L-tyrosine had a more potent effect on T98G-EV cells, reducing their growth by 27%,

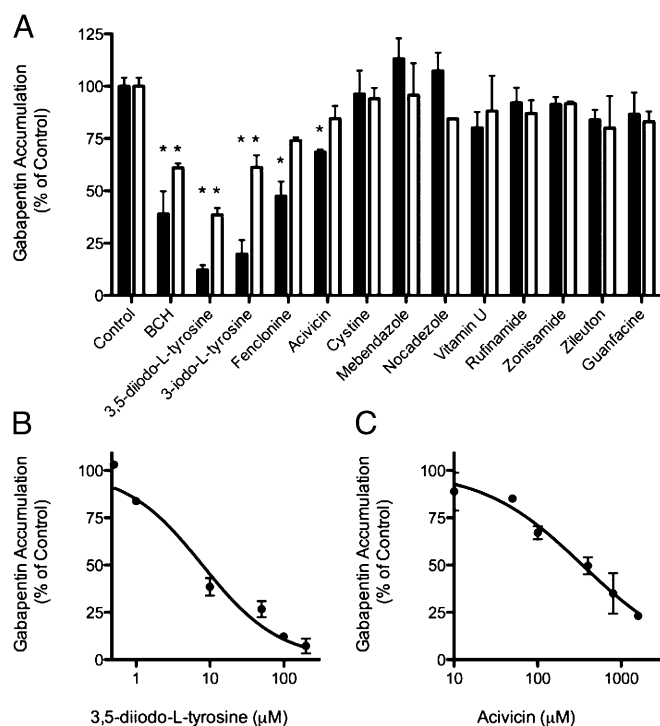


Fig. 3. Experimental validation of predicted LAT-1 ligands. Predicted LAT-1 ligands were validated by *cis*-inhibition of gabapentin uptake. (*A*) Cells were coinoculated with 12 predicted ligands and a positive control (BCH) at either 100 μ M (filled bars) or 10 μ M (open bars) concentrations and gabapentin (1 μ M unlabeled and 10 nM radiolabeled). Each bar depicts the mean of two to four separate experiments; error bars represent SEM. (*B* and *C*) Dose-dependent inhibition of gabapentin (1 μ M unlabeled and 10 nM radiolabeled) accumulation by 3,5-diiodo-L-tyrosine (IC₅₀ = 7.9 μ M) and acivicin (IC₅₀ = 340 μ M), respectively. Each point is the mean of two or three separate experiments; error bars represent SEM. Statistical analysis in *A* was by one-way ANOVA and Dunnett's multiple comparison test. **P* < 0.05.

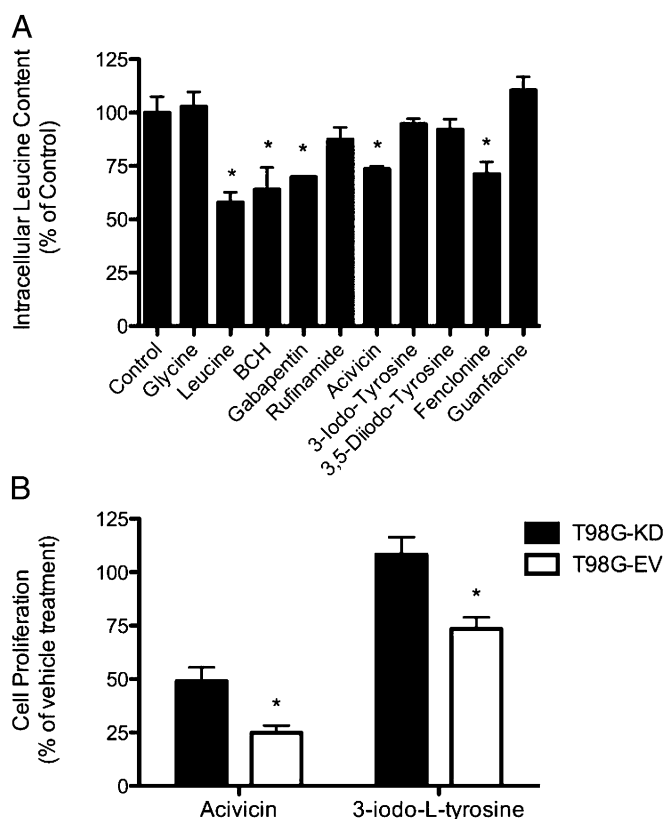


Fig. 4. Substrate determination and cytotoxicity characterization of predicted ligands. Predicted LAT-1 ligands validated in *cis*-inhibition assays were subjected to substrate determination by *trans*-stimulation of L-leucine efflux (1 μ M unlabeled and 10 nM radiolabeled). (A) Cells were preloaded with L-leucine, and efflux was induced by subsequent addition of each test compound at a concentration of 1 mM. Gabapentin, L-leucine, and BCH were included as positive controls, and glycine and guanfacine were included as negative controls. (B) The cytotoxic effects of acivicin (100 μ M) and 3-iodo-L-tyrosine (1 mM) against T98G glioblastoma cells stably expressing an shRNA against LAT-1 (T98G-KD; filled bars) or EV (T98G-EV; open bars) are depicted. Cell proliferation for both cell lines and treatment conditions were normalized to cell density at treatment day 0 and then to the vehicle control treatment at 48 h. Each bar represents the mean of three or four separate experiments, and error bars represent the SEM. Statistical analysis in A was by one-way ANOVA and Dunnett's multiple comparison test and in B was by two-way ANOVA and Bonferroni correction for multiple testing. * $P < 0.05$.

whereas having no effect on T98G-KD (Fig. 4B Right). These results suggest that both 3-iodo-L-tyrosine and acivicin are capable of inhibiting cancer cell proliferation in a LAT-1-dependent manner by means of two distinct mechanisms, including nutrient deprivation and cytotoxicity, respectively.

Discussion

Three key findings emerge from our study. First, two drug-like molecules that interact with different proteins in the CNS are also substrates of LAT-1. This finding may explain the mechanism by which these drugs penetrate the BBB to reach their targets in the CNS. It also provides a starting point for optimizing the two drugs for better BBB permeability. Second, two of the discovered LAT-1 ligands, including one inhibitor and one substrate, inhibit proliferation of cancer cells. This result indicates that LAT-1 can be targeted for cancer therapy by means of different mechanisms and reveals chemical tools for further characterizing the role of LAT-1 in cancer. Third, the identified LAT-1 ligands achieve their pharmacological effect (positive or negative) on the CNS or cancer by interacting with multiple targets.

This finding suggests that effective therapy can be obtained by applying modeling and docking approaches to whole systems, including pathways and networks. We take each of the three key findings in turn.

LAT-1-Mediated BBB Drug Permeability. Passive diffusion has long been thought of as the primary mechanism by which most drugs cross the BBB to permeate the CNS (31). The contribution of carrier-mediated transport to this process is assumed to be minimal, even though different classes of membrane transporters have been shown to restrict and/or facilitate access of drugs, nutrients, and toxins to the CNS (32–34). LAT-1 is one such influx transporter known to transport nutrients and xenobiotics across the BBB. In this study, we identified two previously unknown LAT-1 substrates, including acivicin and fenclofenone, which may also cross the BBB via LAT-1-mediated transport. Both were found to be likely LAT-1 substrates in *trans*-stimulation studies (Fig. 4), and both are known to have pharmacodynamic effects in the CNS. Even though previous studies have used *trans*-stimulation to establish whether or not a specific transporter can transport different compounds (35–37), this assay provides indirect evidence that a compound may be a substrate for a specific transporter. Nevertheless, acivicin was assessed in a clinical trial for treating various solid tumors that did not involve the CNS but failed these trials due to CNS-related toxic side effects (e.g., lethargy and confusion) (38). Furthermore, these side effects were reversed when acivicin was concomitantly administered with a mixture of amino acids, including the prototypical LAT-1 substrate, L-leucine. These observations highly implicate LAT-1 in mediating acivicin's CNS permeability in humans. The second molecule, fenclofenone, is an irreversible tryptophan hydroxylase inhibitor used to deplete CNS serotonin levels in animal models of human disease (39). Together with our results, LAT-1 likely mediates the effects in the CNS by transporting fenclofenone across the BBB. Therefore, influx transporters such as LAT-1 may be important mediators of drug efficacy and toxicity in the CNS and have a greater contribution to drug penetration across the BBB than previously thought.

Targeting LAT-1 for Cancer Therapy. Changes in cell metabolism are strongly associated with cancer. Membrane transporters have been shown to play a key role in such reprogrammed metabolic networks by providing nutrients to transforming cells. For example, the glucose transporter (GLUT1; *SLC2A1*) is up-regulated in various cancers to provide glucose as a carbon source to accommodate an increased rate of anabolic cellular reactions and to maintain a microecosystem favorable for cancer cells (40). Moreover, LAT-1 imports essential amino acids that serve as nutrients and pro-proliferative signaling molecules by exporting glutamine brought into cancer cells via the glutamine transporter ASCT2 (10). Thus, therapeutics targeting LAT-1 can be (i) inhibitors that selectively block transport by LAT-1 and/or ASCT2, depriving the cancer cell of nutrients required for proliferation, or (ii) cytotoxic substrates that are delivered into the cell via LAT-1 and/or ASCT2 to act on an intracellular target. LAT-1 ligands that act through each of these mechanisms were discovered in our screen (Figs. 2–4 and Table 1).

First, 3-iodo-L-tyrosine is a thyroid hormone derivative typically used to treat hormone deficiencies and as a radioactive agent. Here, *cis*-inhibition and cell-proliferation experiments identified 3-iodo-L-tyrosine as a potent LAT-1 inhibitor (Fig. 3A) that reduces proliferation of T98G glioblastoma cells (Fig. 4B), possibly by starving these cells of nutrients supplied by LAT-1. Our results suggest that, in addition to its putative anticancer applications, 3-iodo-L-tyrosine may be useful as a diagnostic imaging agent to identify tumors and other disease states associated with LAT-1 up-regulation (41).

Second, acivicin is a cytotoxic agent with antitumor activity that targets glutamine-dependent amidotransferases in the biosynthesis of purines and pyrimidines (42). *Trans*-stimulation and

followed by addition of 700 μ L of lysis buffer (0.1% SDS vol/vol, 0.1 N NaOH). Intracellular radioactivity was determined as described above.

Cell Proliferation Assay. T98G-KD and -EV cells were seeded at 2.5×10^3 cells per well in 96-well plates (Corning Life Sciences), and on the following day cells were exposed to growth medium containing either drug or vehicle (0.85% saline solution) for 48 h. Cell density was measured on the treatment day and 48 h after treatment by using the CellTiter-Glo cell viability kit (Promega) according to the manufacturer's instructions. Cell lysates were transferred to white opaque 96-well plates (Corning Life Sciences), and bioluminescence was measured on a Glomax luminometer (Promega). Proliferation of each cell line after 48 h was first normalized to the density measured on treatment day (0 h), followed by normalization of drug to vehicle treatment.

1. Kanai Y, et al. (1998) Expression cloning and characterization of a transporter for large neutral amino acids activated by the heavy chain of 4F2 antigen (CD98). *J Biol Chem* 273(37):23629–23632.
2. Roberts LM, et al. (2008) Subcellular localization of transporters along the rat blood-brain barrier and blood-cerebral-spinal fluid barrier by in vivo biotinylation. *Neuroscience* 155(2):423–438.
3. Alexander GM, Schwartzman RJ, Grothusen JR, Gordon SW (1994) Effect of plasma levels of large neutral amino acids and degree of parkinsonism on the blood-to-brain transport of levodopa in naive and MPTP parkinsonian monkeys. *Neurology* 44(8):1491–1499.
4. Wang Y, Welty DF (1996) The simultaneous estimation of the influx and efflux blood-brain barrier permeabilities of gabapentin using a microdialysis-pharmacokinetic approach. *Pharm Res* 13(3):398–403.
5. Killian DM, Hermeling S, Chikhale PJ (2007) Targeting the cerebrovascular large neutral amino acid transporter (LAT1) isoform using a novel disulfide-based brain drug delivery system. *Drug Deliv* 14(1):25–31.
6. Gynther M, et al. (2010) Brain uptake of ketoprofen-lysine prodrug in rats. *Int J Pharm* 399(1–2):121–128.
7. Kaira K, et al. (2008) Prognostic significance of L-type amino acid transporter 1 expression in resectable stage I–III nonsmall cell lung cancer. *Br J Cancer* 98(4):742–748.
8. Kobayashi K, et al. (2008) Enhanced tumor growth elicited by L-type amino acid transporter 1 in human malignant glioma cells. *Neurosurgery* 62(2):493–503, discussion 503–504.
9. Kaira K, et al. (2008) L-type amino acid transporter 1 and CD98 expression in primary and metastatic sites of human neoplasms. *Cancer Sci* 99(12):2380–2386.
10. Nicklin P, et al. (2009) Bidirectional transport of amino acids regulates mTOR and autophagy. *Cell* 136(3):521–534.
11. Oda K, et al. (2010) L-type amino acid transporter 1 inhibitors inhibit tumor cell growth. *Cancer Sci* 101(1):173–179.
12. Ohkawa M, et al. (2011) Oncogenicity of L-type amino-acid transporter 1 (LAT1) revealed by targeted gene disruption in chicken DT40 cells: LAT1 is a promising molecular target for human cancer therapy. *Biochem Biophys Res Commun* 406(4):649–655.
13. Shennan DB, Thomson J (2008) Inhibition of system L (LAT1/CD98hc) reduces the growth of cultured human breast cancer cells. *Oncol Rep* 20(4):885–889.
14. Verrey F, et al. (2004) CATs and HATs: the SLC7 family of amino acid transporters. *Pflügers Arch* 447(5):532–542.
15. Gao X, et al. (2009) Structure and mechanism of an amino acid antiporter. *Science* 324(5934):1565–1568.
16. Shaffer PL, Goehring A, Shankaranarayanan A, Gouaux E (2009) Structure and mechanism of a Na⁺-independent amino acid transporter. *Science* 325(5943):1010–1014.
17. Gao X, et al. (2010) Mechanism of substrate recognition and transport by an amino acid antiporter. *Nature* 463(7282):828–832.
18. Kowalczyk L, et al. (2011) Molecular basis of substrate-induced permeation by an amino acid antiporter. *Proc Natl Acad Sci USA* 108(10):3935–3940.
19. Schlessinger A, et al. (2010) Comparison of human solute carriers. *Protein Sci* 19(3):412–428.
20. Fang Y, et al. (2009) Structure of a prokaryotic virtual proton pump at 3.2 Å resolution. *Nature* 460(7258):1040–1043.
21. Yamashita A, Singh SK, Kawate T, Jin Y, Gouaux E (2005) Crystal structure of a bacterial homologue of Na⁺/Cl[−]-dependent neurotransmitter transporters. *Nature* 437(7056):215–223.
22. Forrest LR, Krämer R, Ziegler C (2011) The structural basis of secondary active transport mechanisms. *Biochim Biophys Acta* 1807(2):167–188.
23. Shi L, Weinstein H (2010) Conformational rearrangements to the intracellular open states of the LeuT and ApCt transporters are modulated by common mechanisms. *Biophys J* 99(12):L103–L105.
24. Jardetzky O (1966) Simple allosteric model for membrane pumps. *Nature* 211(5052):969–970.
25. Guan L, Kaback HR (2006) Lessons from lactose permease. *Annu Rev Biophys Biomol Struct* 35:67–91.
26. Shen MY, Sali A (2006) Statistical potential for assessment and prediction of protein structures. *Protein Sci* 15(11):2507–2524.
27. Eramian D, Eswar N, Shen MY, Sali A (2008) How well can the accuracy of comparative protein structure models be predicted? *Protein Sci* 17(11):1881–1893.
28. Schlessinger A, et al. (2011) Structure-based discovery of prescription drugs that interact with the norepinephrine transporter, NET. *Proc Natl Acad Sci USA* 108(38):15810–15815.

Statistical Analysis. Data were analyzed by one-way ANOVA followed by Dunnett's multiple comparison test, two-way ANOVA followed by Bonferroni correction for multiple testing, or two-tailed unpaired *t* test. Probability values of <0.05 were considered statistically significant.

ACKNOWLEDGMENTS. We thank Ursula Pieper, Ben Webb, and Elina Tjioe for technical assistance and maintenance of the computational resources required for this study; Jonathan Socklosky for technical assistance in cloning LAT-1; and University of California, San Francisco ViraCore for the production of custom lentivirus. The project was supported by National Institutes of Health Grants R01 GM54762 (to A. Sali), U54 GM074929 and U01 GM61390 (to A. Sali and K.M.G.), P01 GM71790 (to A. Sali), F32 GM088991 (to A. Schlessinger), and T32 GM007175 (to E.G.G.). We also received funding for computing hardware from Hewlett Packard, IBM, NetApps, Intel, Ron Conway, and Mike Homer.

29. Huang N, Shoichet BK, Irwin JJ (2006) Benchmarking sets for molecular docking. *J Med Chem* 49(23):6789–6801.
30. Fan H, et al. (2009) Molecular docking screens using comparative models of proteins. *J Chem Inf Model* 49(11):2512–2527.
31. Mensch J, Oyarzabal J, Mackie C, Augustijns P (2009) In vivo, in vitro and in silico methods for small molecule transfer across the BBB. *J Pharm Sci* 98(12):4429–4468.
32. Smith BJ, et al. (2001) P-glycoprotein efflux at the blood-brain barrier mediates differences in brain disposition and pharmacodynamics between two structurally related neurokinin-1 receptor antagonists. *J Pharmacol Exp Ther* 298(3):1252–1259.
33. Park S, Sinko PJ (2005) The blood-brain barrier sodium-dependent multivitamin transporter: a molecular functional in vitro-in situ correlation. *Drug Metab Dispos* 33(10):1547–1554.
34. Abbott NJ, Patabendige AA, Dolman DE, Yusof SR, Begley DJ (2010) Structure and function of the blood-brain barrier. *Neurobiol Dis* 37(1):13–25.
35. Yamamoto A, Akanuma S, Tachikawa M, Hosoya K (2010) Involvement of LAT1 and LAT2 in the high- and low-affinity transport of L-leucine in human retinal pigment epithelial cells (ARPE-19 cells). *J Pharm Sci* 99(5):2475–2482.
36. Zhang L, Schaner ME, Giacomini KM (1998) Functional characterization of an organic cation transporter (hOCT1) in a transiently transfected human cell line (HeLa). *J Pharmacol Exp Ther* 286(1):354–361.
37. Meier C, Ristic Z, Klauser S, Verrey F (2002) Activation of system L heterodimeric amino acid exchangers by intracellular substrates. *EMBO J* 21(4):580–589.
38. Hidalgo M, et al. (1998) A Phase I and pharmacological study of the glutamine antagonist acivicin with the amino acid solution aminosyn in patients with advanced solid malignancies. *Clin Cancer Res* 4(11):2763–2770.
39. Delaville C, Navailles S, Benazzouz A (2012) Effects of noradrenaline and serotonin depletions on the neuronal activity of globus pallidus and substantia nigra pars reticulata in experimental parkinsonism. *Neuroscience* 202:424–433.
40. Kroemer G, Pouyssegur J (2008) Tumor cell metabolism: cancer's Achilles' heel. *Cancer Cell* 13(6):472–482.
41. Lahoutte T, et al. (2003) Comparative biodistribution of iodinated amino acids in rats: selection of the optimal analog for oncologic imaging outside the brain. *J Nucl Med* 44(9):1489–1494.
42. O'Dwyer PJ, Alonso MT, Leyland-Jones B (1984) Acivicin: a new glutamine antagonist in clinical trials. *J Clin Oncol* 2(9):1064–1071.
43. Bonomi P, Finkelstein D, Chang A (1994) Phase II trial of acivicin versus etoposide-cisplatin in non-small cell lung cancer. An Eastern Cooperative Oncology Group study. *Am J Clin Oncol* 17(3):215–217.
44. Schlessinger A, et al. (2012) High selectivity of the γ -aminobutyric acid transporter 2 (GAT-2, SLC6A13) revealed by structure-based approach. *J Biol Chem* 287(45):37745–37756.
45. Pei J, Kim BH, Grishin NV (2008) PROMALS3D: a tool for multiple protein sequence and structure alignments. *Nucleic Acids Res* 36(7):2295–2300.
46. Sali A, Blundell TL (1993) Comparative protein modelling by satisfaction of spatial restraints. *J Mol Biol* 234(3):779–815.
47. Krivov GG, Shapovalov MV, Dunbrack RL, Jr. (2009) Improved prediction of protein side-chain conformations with SCWRL4. *Proteins* 77(4):778–795.
48. Carlsson J, et al. (2011) Ligand discovery from a dopamine D3 receptor homology model and crystal structure. *Nat Chem Biol* 7(11):769–778.
49. Kyte J, Doolittle RF (1982) A simple method for displaying the hydropathic character of a protein. *J Mol Biol* 157(1):105–132.
50. Ashkenazy H, Erez E, Martz E, Pupko T, Ben-Tal N (2010) ConSurf 2010: calculating evolutionary conservation in sequence and structure of proteins and nucleic acids. *Nucleic Acids Res* 38(Web Server issue):W529–W533.
51. Mysinger MM, Shoichet BK (2010) Rapid context-dependent ligand desolvation in molecular docking. *J Chem Inf Model* 50(9):1561–1573.
52. Overington J (2009) ChEMBL. An interview with John Overington, team leader, chemogenomics at the European Bioinformatics Institute Outstation of the European Molecular Biology Laboratory (EMBL-EBI). Interview by Wendy A. Warr. *J Comput Appl Mol Des* 23(4):195–198.
53. Apweiler R, et al. (2010) The Universal Protein Resource (UniProt) in 2010. *Nucleic Acids Res* 38(Database issue):D142–D148.
54. Wang X, McManus M (2009) Lentivirus production. *J Vis Exp* (32):e1499.
55. Chen Y, Zhang S, Sorani M, Giacomini KM (2007) Transport of paraquat by human organic cation transporters and multidrug and toxic compound extrusion family. *J Pharmacol Exp Ther* 322(2):695–700.

Supporting Information

Geier et al. 10.1073/pnas.1218165110

SI Materials and Methods

Template Selection. To identify potential templates for modeling LAT-1, we used fold-recognition and modeling servers HHpred (1) and I-Tasser (2), and we also analyzed the LAT-1 entries in the database of comparative protein structure models ModBase (3) and the Transporter Classification Database (4). These computational tools revealed that LAT-1 exhibits significant sequence similarity to protein structures in the amino acid/polyamine/organocation (APC) superfamily of the Orientations of Proteins in Membranes database (5). To select the optimal template for structure-based ligand discovery, we used the following considerations: (i) sequence similarity to LAT-1, (ii) structure quality, and (iii) conformation, including whether it is ligand-bound or not, and whether the structure is in an occluded, inward-facing, or outward-facing conformation.

LAT-1–AdiC Alignment. We used a published alignment (6) and alignments obtained from the Promals3D server (7). Briefly, Promals3D relies on multiple protein sequences as well as predicted secondary structure and information derived from homologs with 3D structures. Gaps were present mainly in the predicted extracellular loops and were manually refined (Fig. S1). However, in our final alignments, there were also gaps within the predicted and observed transmembrane helices (TMHs) of LAT-1 and AdiC, respectively. They included short insertions of one to three residues within TMHs of LAT-1 (i.e., in TMH1, TMH3, and TMH4), which probably occurred because the TMHs of LAT-1 are predicted to be longer than those of the AdiC. One of these insertions (i.e., Gln-145) is located near the predicted binding site and might affect its conformation. In addition, two of the gaps were longer deletions in TMH9 and TMH10 of LAT-1. These TMHs are more divergent in sequence between AdiC and LAT-1, making the alignment in these regions unreliable; however, they are relatively far away from the binding site (~15 Å) and are unlikely to have a significant effect on the binding site conformation and docking results.

Residue Conservation and Hydrophobicity Analysis. Evolutionary conservation was calculated by using the ConSurf server (<http://consurf.tau.ac.il/>) (8). For the LAT-1 model, we used the default parameters. The conservation values for the AdiC structure were not assigned for all of the residues using a variety of similarity cutoffs and databases, probably because prokaryotic proteins in this family are highly divergent in sequence (9). Thus, for the AdiC structure, we used the cutoff on sequence identity of 20%, the cutoff on the E-value of 0.1, and the UniProt database. The computed conservation values were mapped onto the LAT-1 model and the template structure by using Chimera (10), using the scripts provided by the ConSurf server. The hydrophobicity profile was computed by using Chimera, relying on the Kyte–Doolittle hydrophobicity scale (11).

The conservation and hydrophobicity profiles are generally similar in the LAT-1 model and the AdiC structure, further confirming the model. The minor differences in the hydrophobicity profiles of LAT-1 and AdiC can be partially explained by the differences in their binding partners. For example, LAT-1 binds the single transmembrane protein SLC3A2, whereas AdiC is not known

to be involved in a similar interaction. Finally, hydrophobic and nonconserved positions are usually predicted to face the estimated location of the lipid membrane, whereas conserved and hydrophilic residues are modeled in the core, where they may be involved in helix–helix interactions and ligand recognition (12, 13). In contrast, the conservation profile on the surface of the experimentally determined AdiC structure does not give such a clear signal, possibly because it is involved in protein–protein interactions.

Selection of Molecules for Experimental Testing. The 200 (3.1%) KEGG DRUG and 500 (3.9%) KEGG COMPOUND highest-ranking hits of the four computational screens (i.e., two datasets against two models) were analyzed manually. In particular, we examined similarities of the docking poses of these ligands to those in the predicted complexes of LAT-1 with known ligands. Additionally, we discarded top-ranked hits for several reasons (14–16): (i) likely false positives related to the limitation of the docking programs, including docking poses with high internal energies or unbound polar groups; (ii) compounds that are not purchasable or too expensive; (iii) compounds that are not novel, because we tried to balance between chemically novel molecules and those that are pharmacologically interesting but might not exhibit novel chemistry.

LAT-1 mRNA Expression. LAT-1 expression was measured as described (17). Briefly, total RNA was isolated from cells plated in six-well plates (Corning Life Sciences) with the Qiagen RNeasy RNA Isolation Kit per the manufacturer's protocol and stored at –80 °C until use. Reverse-transcriptase PCR was performed on 2 µg of total RNA by using the Invitrogen SuperScript VILO cDNA Synthesis Kit per the manufacturer's protocol to create a cDNA library. The resulting cDNA was used as a template for quantitative real-time PCR (qRT-PCR) using TaqMan Gene Expression Assays for human LAT-1 (Assay ID: Hs01001190_m1) and human GAPDH (Assay ID: Hs99999905_m1). qRT-PCR reactions were carried out in 96-well reaction plates in a volume of 10 µL by using the TaqMan Fast Universal Master Mix (Applied Biosystems). Reactions were run on the Applied Biosystems 7500 Fast Real-Time PCR System with the following profile: 95 °C for 20 s followed by 40 cycles of 95 °C for 3 s and 60 °C for 30 s. The relative expression of each mRNA was calculated by the comparative $\Delta\Delta C_t$ method.

LAT-1 Kinetic Studies. The kinetics of L-leucine uptake in HEK-LAT1 cells were determined as described (18). Briefly, varying amounts of unlabeled L-leucine were added to the uptake solutions to give increasing total ($[^3H]$ plus unlabeled L-leucine) substrate concentrations, ranging from 1 to 300 µM at 37 °C. Nonspecific cell-associated radioactivity was determined by measuring substrate uptake at 4 °C at each substrate concentration, and these values were then subtracted from the results at 37 °C LAT-1–transfected cells to give the final kinetic data. The K_m and V_{max} values were obtained by fitting the Michaelis–Menten equation $V = V_{max} \times [S]/(K_m + [S])$ using GraphPad Prism (Version 5.0), where V refers to the rate of substrate transport, V_{max} refers to the maximum rate of substrate transport, $[S]$ refers to the concentration of substrate, and K_m is defined as the concentration of substrate at the half-maximal transport rate.

1. Soding J, Biegert A, Lupas AN (2005) The HHpred interactive server for protein homology detection and structure prediction. *Nucleic Acids Res* 33(Web Server issue):W244–W248.
2. Zhang Y (2008) I-TASSER server for protein 3D structure prediction. *BMC Bioinformatics* 9:40.

3. Pieper U, et al. (2011) ModBase, a database of annotated comparative protein structure models, and associated resources. *Nucleic Acids Res* 39(Database issue):D465–D474.
4. Saier MH, Jr., Yen MR, Noto K, Tamang DG, Elkan C (2009) The Transporter Classification Database: recent advances. *Nucleic Acids Res* 37(Database issue):D274–D278.

- Lomize MA, Lomize AL, Pogozheva ID, Mosberg HI (2006) OPM: orientations of proteins in membranes database. *Bioinformatics* 22(5):623–625.
- Gao X, et al. (2009) Structure and mechanism of an amino acid antiporter. *Science* 324(5934):1565–1568.
- Pei J, Kim BH, Grishin NV (2008) PROMALS3D: a tool for multiple protein sequence and structure alignments. *Nucleic Acids Res* 36(7):2295–2300.
- Ashkenazy H, Erez E, Martz E, Pupko T, Ben-Tal N (2010) ConSurf 2010: calculating evolutionary conservation in sequence and structure of proteins and nucleic acids. *Nucleic Acids Res* 38(Web Server issue):W529–W533.
- Schlessinger A, et al. (2010) Comparison of human solute carriers. *Protein Sci* 19(3): 412–428.
- Pettersen EF, et al. (2004) UCSF Chimera—a visualization system for exploratory research and analysis. *J Comput Chem* 25(13):1605–1612.
- Kyte J, Doolittle RF (1982) A simple method for displaying the hydropathic character of a protein. *J Mol Biol* 157(1):105–132.
- Illergård K, Kauko A, Elofsson A (2011) Why are polar residues within the membrane core evolutionary conserved? *Proteins* 79(1):79–91.
- Fleishman SJ, Ben-Tal N (2006) Progress in structure prediction of alpha-helical membrane proteins. *Curr Opin Struct Biol* 16(4):496–504.
- Kuntz ID (1992) Structure-based strategies for drug design and discovery. *Science* 257(5073):1078–1082.
- Shoichet BK (2004) Virtual screening of chemical libraries. *Nature* 432(7019):862–865.
- Carlsson J, et al. (2011) Ligand discovery from a dopamine D3 receptor homology model and crystal structure. *Nat Chem Biol* 7(11):769–778.
- More SS, et al. (2011) Vorinostat increases expression of functional norepinephrine transporter in neuroblastoma in vitro and in vivo model systems. *Clin Cancer Res* 17(8):2339–2349.
- Chen Y, Zhang S, Sorani M, Giacomini KM (2007) Transport of paraquat by human organic cation transporters and multidrug and toxic compound extrusion family. *J Pharmacol Exp Ther* 322(2):695–700.

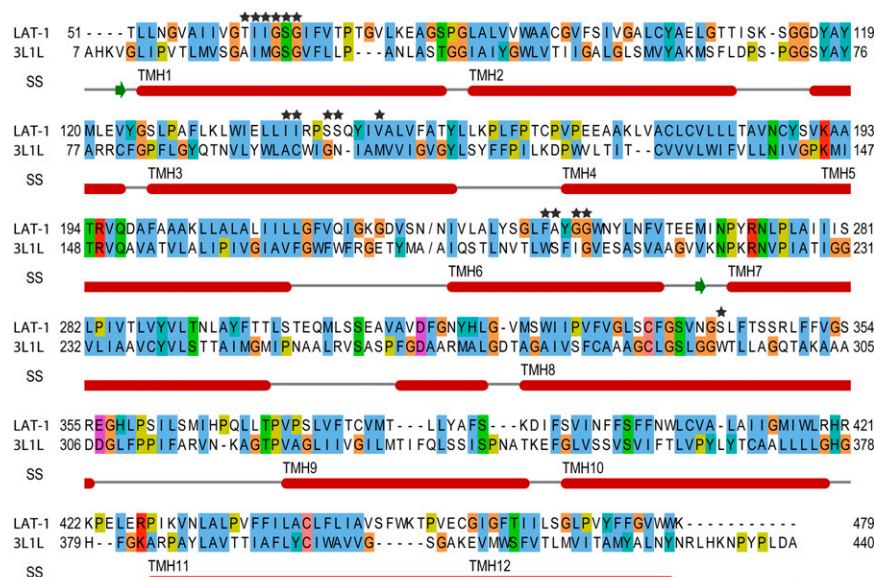


Fig. S1. LAT-1–AdiC alignment. The sequence alignment was visualized by using Jalview (1). The aligned residues are colored based on their type using the Clustlx color scheme. The template structure (Protein Data Bank ID code 3L1L) helical and strand segments are indicated with red rectangles and green arrows, respectively. The transmembrane helices (TMHs) of 3L1L were defined by using the PPM server (2); the remainder of the secondary structure segments (SS) were defined by the DSSP program (3). The residues that are important for LAT-1 ligand binding according to our model are highlighted with gray stars. The LAT-1 loop that was excluded from modeling is marked with /.

- Clamp M, Cuff J, Searle SM, Barton GJ (2004) The Jalview Java alignment. *Bioinformatics* 20(3):426–427.
- Lomize MA, Pogozheva ID, Joo H, Mosberg HI, Lomize AL (2012) OPM database and PPM web server: Resources for positioning of proteins in membranes. *Nucleic Acids Res* 40(Database issue):D370–D376.
- Kabsch W, Sander C (1983) Dictionary of protein secondary structure: Pattern recognition of hydrogen-bonded and geometrical features. *Biopolymers* 22(12):2577–2637.

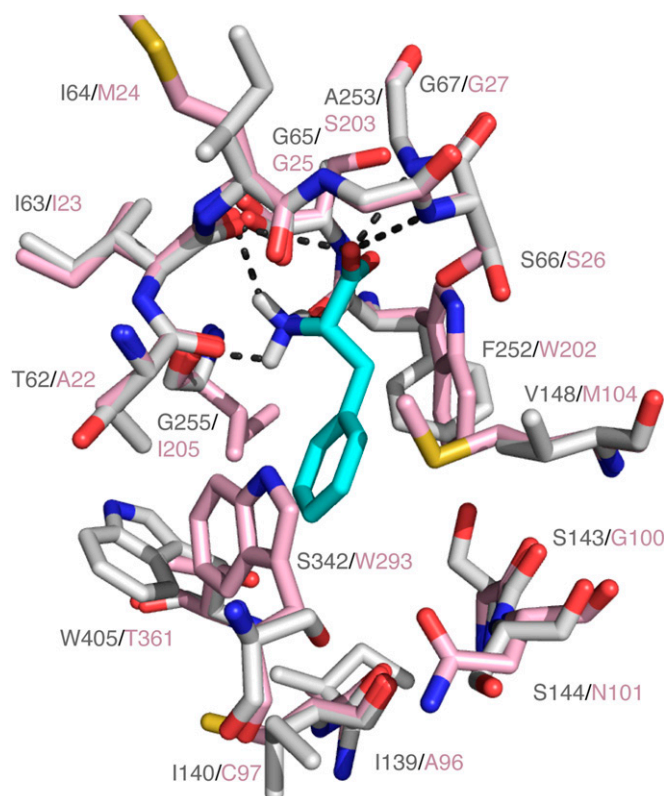


Fig. S2. Binding sites of LAT-1 and AdiC. LAT-1 model (light gray) is superposed on the X-ray structure of AdiC (pink). All other protein atoms are illustrated by sticks; oxygen, nitrogen, and sulfur atoms are colored in red, purple, and yellow, respectively. Phenylalanine, a substrate of LAT-1, is depicted in cyan sticks, and its predicted hydrogen bonds with LAT-1 (involving residues T62, I63, I64, S66, G67, F252, A253, and G255) are shown as dotted gray lines.

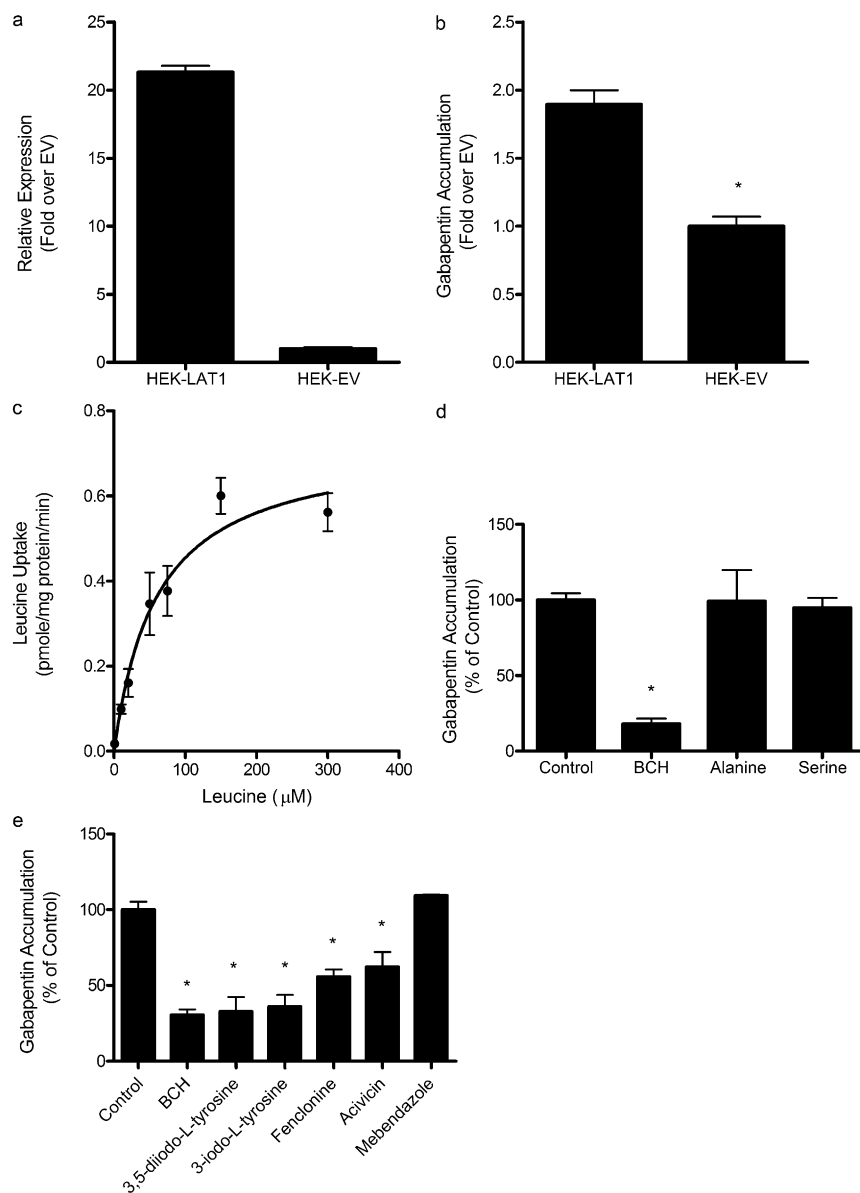


Fig. S3. Validation of LAT-1 function in HEK-LAT1 cells. (A) Overexpression of LAT-1 in transfected HEK-LAT1 cells relative to EV cells. (B) Validation of LAT-1 function in LAT-1-transfected cells. Gabapentin (1 μ M unlabeled and 10 nM radiolabeled) uptake in HEK-LAT1 cells was approximately twofold higher than in EV cells. (C) Kinetics of L-leucine uptake in HEK-LAT1 cells. L-leucine uptake was measured at 1, 10, 20, 50, 75, 150, and 300 μ M, and the curve was fit to the Michaelis-Menten equation to obtain a K_m value of 60.63 ± 13.05 μ M. (D) Distinguishing LAT-1 from LAT-2 uptake of gabapentin in HEK-LAT1 cells by *cis*-inhibition with L-alanine. Cells were coincubated with gabapentin and either 1 mM 2-aminobicyclo-(2,2,1)-heptane-2-carboxylic acid (BCH; LAT-1 and LAT-2 inhibitor), L-alanine (LAT-2 inhibitor), or L-serine (negative control). BCH reduced intracellular gabapentin accumulation by ~83%, whereas L-alanine and -serine were not able to inhibit intracellular gabapentin accumulation. (E) Predicted LAT-1 ligands were validated by *cis*-inhibition of L-leucine uptake in HEK-LAT1 cells. Cells were coincubated with L-leucine (1 μ M unlabeled and 10 nM radiolabeled) and predicted ligands at 100 μ M concentration. BCH is included as a positive control. Each point is the mean of two or three separate experiments; error bars represent SEM. Statistical analysis was by one-way ANOVA and Dunnett's multiple comparison test in D and E and by two-tailed unpaired *t* test in B. **P* < 0.05.

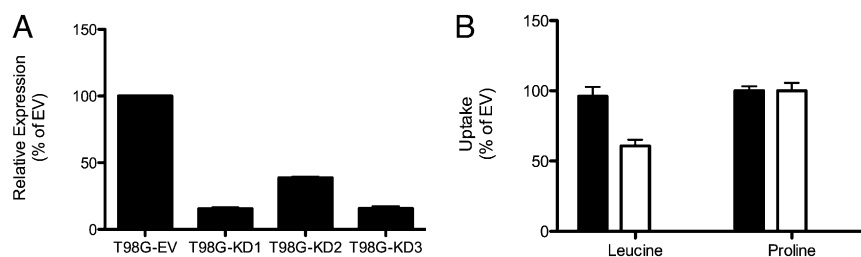


Fig. S4. Validation of LAT-1 knockdown in T98G glioblastoma cells. (A) Reduced LAT-1 mRNA in T98G cells expressing three different anti-LAT-1 shRNAs. T98G-KD1 and -KD3 both showed ~85% reduction in LAT-1 mRNA. (B) Functional validation of LAT-1 knockdown was determined by measuring cellular L-leucine and -proline (1 μ M unlabeled and 10 nM radiolabeled) accumulation in T98G-KD1 (T98G-KD in main text; open bars) and T98G-EV (filled bars) cells under the conditions described in *Materials and Methods* (uptake incubation time was 1 min). T98G-KD cells accumulated ~40% less L-leucine, a prototypical LAT-1 substrate, than T98G-EV cells, whereas both cell lines accumulated similar amounts of the non-LAT-1 substrate L-proline.

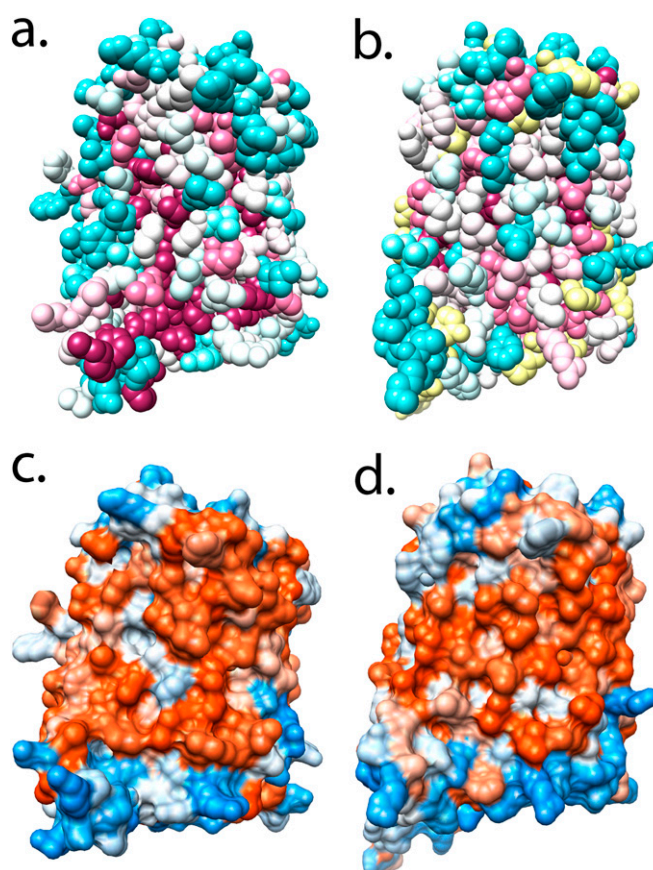


Fig. S5. Conservation and hydrophobicity profiles for the LAT-1 model and the AdiC structure. Side views of the LAT-1 model and the AdiC structure are shown. (A and B) Evolutionary conservation grades (from 1 to 9) are mapped onto the surface of the LAT-1 model (A) and the AdiC structure (B); the residue positions are colored in cyan for most variable, to white, and to maroon for most conserved; unassigned positions are colored yellow. (C and D) Hydrophobicity values are mapped onto the surface of the LAT-1 model (C) and the AdiC structure (D); the residues are colored in blue for the most hydrophilic, to white, and to orange for the most hydrophobic.

Table S3. Anti-LAT-1 shRNA sequences

| Cell line* | Position [†] | Sequence [‡] |
|------------|-----------------------|-----------------------|
| T98G-KD1 | 3861 | GAAAGTAGCTGCTAGTGAA |
| T98G-KD2 | 4294 | GCTAACGTCTTACTAATTT |
| T98G-KD3 | 4512 | GTTAATGGCTAACCTGTTA |

*Name given to T98G glioblastoma cells stably expressing a given shRNA construct.

[†]Position indicates the first base pair within the human SLC7A5 mRNA sequence each shRNA targets.

[‡]Sequence of each construct targeting LAT-1 mRNA.